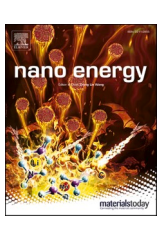


Contents lists available at ScienceDirect

Nano Energy

journal homepage: www.elsevier.com/locate/nanoen





Inherent inhibition of oxygen loss by regulating superstructural motifs in anionic redox cathodes

Jiajie Liu^{a,1}, Rui Qi^{a,1}, Changjian Zuo^a, Cong Lin^a, Wenguang Zhao^a, Ni Yang^a, Jianyuan Li^a, Junliang Lu^a, Xin Chen^a, Jimin Qiu^a, Mihai Chu^a, Mingjian Zhang^a, Cheng Dong^a, Yinguo Xiao^a, Haibiao Chen^{b,*}, Feng Pan^{a,*}

ARTICLE INFO

Keywords: Sodium layered oxide Anionic redox Superstructural motif In-plane Mn migration Oxygen loss

ABSTRACT

The capacity of the layered oxide cathode in a sodium ion battery can be increased by harnessing anionic redox. However, the extra capacity induced by anionic redox comes at the expense of reversibility due to the irreversible oxidation and subsequent loss of oxygen. Here, we report a universal strategy of improving the reversibility of oxygen redox in sodium layered oxides by regulating the superstructural motifs. The intrinsic chemical properties of superstructural motifs can be directionally altered by modulating the interionic interactions, and the rational integration of selected superstructural motifs can result in advanced materials with target performance. As a demonstration, a novel cathode comprising both $Mg@Mn_6$ and $Li@Mn_6$ superstructural motifs is designed and synthesized with inherently inhibited oxygen loss and significantly improved cyclic reversibility. Detailed characterizations on the atomic-level structure and chemistry of materials revealed that the pinning effect of the $Mg@Mn_6$ superstructural motif is critical to maintain a stable layered structure. The findings from this work open up new routes for the design and development of next-generation high energy cathodes with target performance.

1. Introduction

The ever-increasing demand for universal energy availability at lower costs and better sustainability has driven the quest for new battery chemistries. Sodium ion battery (SIB) is a promising candidate for the next-generation energy storage and an alternative to lithium ion battery (LIB) due to the high abundance, easy availability, and low cost of sodium [1,2]. However, the energy density of current SIB (below 120 Wh kg⁻¹) is still much lower than that of the commercially mature LIB (approaching 300 Wh kg⁻¹) [3-5]. The low energy density of SIBs is mostly limited by the low capacity of the cathode. For conventional intercalation-type cathodes in SIBs, the upper limit of the capacity is dictated by the redox of the metal cations induced by the insertion/extraction of the Na⁺ ions. To gain extra capacity, a new strategy by harnessing the redox of the anions in the cathode has proven to be effective in recent years [6]. The first work on enabling anionic redox in SIB cathodes was reported in 2014 by Komaba's group, using a similar strategy previously applied to Li-rich layered oxides in LIBs. The new

cathode material was produced by introducing Li⁺ into the transition metal (TM) layer in Na-layered oxides (Na_xTMO₂, x < 1) and the resulted P2-type Na_{5/6}Li_{1/4}Mn_{3/4}O₂ exhibited superior capacity over the traditional layered oxides which solely relied on the redox of TM cations [7]. This pioneering work inspired the discovery of a family of analogue materials, e. g., P3-Na_{0.6}Li_{0.2}Mn_{0.8}O₂ [8], P2-Na_{0.72}Li_{0.24}Mn_{0.76}O₂ [9], $P2-Na_{5/6}Li_{5/18}Mn_{13/18}O_2$ [10], and $O3-NaLi_{1/3}Mn_{2/3}O_2$ [11]. In this class of materials, the coordination environment of the $\mathrm{O}^{2\text{-}}$ anions in the TM layer is altered by the introduction of the Li⁺. Some of the O²⁻ anions are coordinated in a way that each O2- is coordinated with one Li+ and two TM cations. Since the interaction between O2- and Li+ is weaker than that between O2- and an TM cation, the O2- anions coordinated with both Li and TM cations can lose electrons more easily than the O²⁻ anions coordinated with only TM cations. As a result, the O2- anions with Li coordination will be able to undergo oxidation and supply additional capacity at a high voltage during charging [12]. The anionic redox of oxygen has greatly promoted the sodium storage capacity of layered oxides. For instance, P2-Na_{0.72}Li_{0.24}Mn_{0.76}O₂ delivered hitherto the

^a School of Advanced Materials, Peking University, Shenzhen Graduate School, Shenzhen 518055, China

^b Institute of Marine Biomedicine, Shenzhen Polytechnic, Shenzhen 518055, China

^{*} Corresponding authors.

E-mail addresses: chenhb@szpt.edu.cn (H. Chen), panfeng@pkusz.edu.cn (F. Pan).

¹ These authors contributed equally to this work.

highest capacity (270 mAh g $^{-1}$) and the highest energy density (700 Wh kg $^{-1}$) in Na-layered oxides. Similar strategies by introducing Mg $^{2+}$ [13, 14], Zn $^{2+}$ [15,16], and TM-vacancies [17–19] into the TM layer followed the same principle in terms of chemistry, and have been proved to be effective as well.

Although anionic redox can significantly improve the capacity of Nalayered oxides, the cycling stability of the cathode remains an major issue to resolve [9]. First, the oxidized O species in the cathode are thermodynamically unstable, and they can either react with the electrolyte components or form fugitive O2. The loss of oxygen from the cathode is detrimental to the structural integrity and should be avoided by all means [20-22]. Second, Li⁺ in the TM layer is not strongly restrained by O^{2} , and can migrate to the alkali metal (AM) layer upon deep charge, leaving abundant vacancies in the TM layer [7,23,24]. Recent studies revealed that these vacancies tend to cluster in order to reach a thermodynamically stable state, accompanied by massive in-plane TM migrations [25,26]. The lattice O ions previously coordinated with at least two TM cations become uncoordinated due to the aggregation of vacancies, and thus form O₂ molecules in the trap. Trapped O₂ molecules could be released upon cycling and leave abundant O-vacancies in the bulk, triggering further TM migration and subsequent structural collapse. Therefore, stabilizing O in the structure is the key to maintain the structural integrity, and should be an effective solution to improve the cycling performance of anionic redox involved Na-layered oxides. Previous researches revealed that Mg ions are effective in adjusting the redox behavior of lattice O and are beneficial for stabilizing the structure of layered oxide cathodes [27-29]. Recently, House et al. [26] reported a method by tuning the superstructure for this purpose. By replacing the honeycomb superstructure with a ribbon superstructure, the aggregation of vacancies was retarded and the reversibility of the cathode was greatly improved. However, the capacity of their more stable cathode with a ribbon-ordered superstructure was only 115 mAh g^{-1} .

In this work, we aim to demonstrate a novel strategy that by regulating the superstructural motifs (SMs) in Na-layered oxides, O in the structure can be stabilized and O loss can be inherently inhibited. Meanwhile, the high capacity of anionic redox cathodes can be retained with improved reversibility. To demonstrate this concept, we start from considering the intrinsic chemical properties of SMs, which can be directionally altered by modulating the ionic interactions within SMs. The rational integration of suitable SMs can result in advanced materials with target performance. As a result, two selected SMs (Li@Mn6 and Mg@Mn₆) with diverse O redox activity and ion mobilities are integrated to yield NLMMOs ($Na_{0.73}Li_{0.23-x}Mg_xMn_{0.77}O_2$, x = 0.06 or 0.12) as a model system. Meanwhile, NLMO (Na_{0.73}Li_{0.23}Mn_{0.77}O₂) containing only the Li@Mn₆ SM is also designed as the control group. In NLMMOs, the Mg@Mn₆ SMs are chemically more stable than the Li@Mn₆ SMs and they serve as pins in the TM layer to suppress the in-plane TM migration and the consequent aggregation of vacancies. We demonstrated that in NLMMOs with regulated superstructures, the irreversible O loss was inhibited and the cycling stability of the cathode was promoted. Through detailed characterizations, a complete logical chain from the atomic-level understanding of SMs to the macroscopical electrochemical performance was created to verify the feasibility of the SM regulating strategy. We propose a concept that superstructure can be modulated by employing various SMs to improve the reversibility of anionic redox cathodes. Our exploration of the structural chemistry in anionic redox cathodes can bring new opportunities for developing better materials as stable and high capacity cathodes for future batteries.

2. Results and discussions

2.1. Structures of NLMO and NLMMOs

To verify the concept, three P2-type layered oxides, $Na_{0.73}Li_{0.23}Mn_{0.77}O_2$ (denoted as NLMO), $Na_{0.73}Li_{0.17}Mg_{0.06}Mn_{0.77}O_2$

(denoted as NLMMO-1/4), and Na $_{0.73}$ Li $_{0.11}$ Mg $_{0.12}$ Mn $_{0.77}$ O $_{2}$ (denoted as NLMMO-1/2), were designed. The ideal in-plane structures of NLMO, NLMMO-1/4, and NLMMO-1/2 are schematically illustrated in Fig. 1a, b, and c, respectively. The Mn ions in the TM layer of NLMO are arranged in a honeycomb pattern with Li $^+$ ions at the centers of all hexagons, constituting Li@Mn $_6$ SMs. When the Mg@Mn $_6$ SMs are incorporated into the structure, the honeycomb ordering of Mn ions remains with some of the Li $^+$ ions at the centers of the hexagons replaced by Mg $^{2+}$ ions, with the total number of SMs being unchanged. Specifically, in the case of NLMMO-1/4, a quarter of Li@Mn $_6$ SMs are replaced by Mg@Mn $_6$ SMs while in the case of NLMMO-1/2, a half of Li@Mn $_6$ SMs are replaced by Mg@Mn $_6$. In these three ideal structures, the stoichiometric contents of Na and Mn are the same, but the relative contents of Li and Mg are varied.

Experimentally, NLMO, NLMMO-1/4, and NLMMO-1/2 were synthesized using a sol-gel method. Detailed procedure of the synthesis is described in the supplementary information. The actual chemical compositions were determined by inductively coupled plasma-atomic emission spectrometry (ICP-AES), and they comply well with the design (Table S1). Scanning electron microscopy (SEM) revealed that the as-synthesized NLMO and NLMMOs samples consisted of micrometer-sized particles, and the NLMO particles were rod-like while the NLMMO particles were plate-like (Fig. S1). Energy-dispersive spectroscopy (EDS) mapping verified that all elements were uniformly distributed throughout the particles in all three materials (Fig. S1). Powder X-ray diffraction (XRD) was conducted to examine the structural consistency of the as-prepared materials. As shown in Fig. 1d, all three materials exhibit the characteristic diffraction patterns of the P2-phase (the structure in Fig. 1g). The shift of the (002) peak towards a lower angle with the increase of Mg content indicates that the incorporation of Mg@Mn6 SM induced a gradual solid-solution process instead of an abrupt phase-transition (Fig. 1e). Rietveld refinements further confirmed the formation of solid solutions in NLMMOs since the refined patterns of the three materials were quite consistent (Fig. 1, h-j). More detailed refinement results show a clear increase in the lattice parameters with the increase of Mg content (Tables S2-S4). The structural consistency between the materials can also be confirmed by the superlattice peaks, which originated from the honeycomb ordering of Mn ions in the TM layer (Fig. 1f) [7]. The characterization results demonstrate that NLMO, NLMMO-1/4, and NLMMO-1/2 were successfully synthesized as designed, with designated chemical compositions and similar crystal structures, laving the groundwork for further investigation on the effect of O loss on the electrochemical behavior of this model system.

2.2. Electrochemical performance of NLMO and NLMMOs

The introduction of Mg@Mn₆ SMs into NLMO was found to result in significant alteration in the electrochemical performance. As shown in Fig. 2a, the voltage profiles of all three materials exhibit a typical plateau corresponding to major O oxidation and minor Mn oxidation during the first charge. The initial charge capacities at a current density of 10 mA g $^{-1}$ and a cutoff voltage of 4.5 V were 223 mAh g $^{-1}$, 191 mAh g $^{-1}$, and 169 mAh g $^{-1}$ for NLMO, NLMMO-1/4, and NLMMO-1/2, respectively. Based on the X-ray photoelectron spectroscopy (XPS) result (Fig. S2), the oxidation number of Mn in NLMMO-1/2 increased from +3.79 to +4 at 4.5 V, indicating that Mn oxidation happened during the initial charge in this series of materials. Therefore, the capacity contributions from Mn oxidation were estimated to be 12 mAh g⁻¹ (0.04 e⁻), 29 mAh g⁻¹ (0.10 e⁻), and 45 mAh g⁻¹ (0.16 e⁻), while those from O oxidation were estimated to be 211 mAh g⁻¹, 162 mAh g⁻¹, and 124 mAh g⁻¹ for NLMO, NLMMO-1/4, and NLMMO-1/2, respectively. The decreased charge capacities in NLMMOs can be attributed to the lower O redox activity in the Mg@Mn6 SMs, which stems from the lower electron density of O²- in the Na-O-Mg configuration due to the stronger Mg²⁺-O²⁻ interaction. The initial discharge capacities at the cutoff voltage of 2.0 V for NLMO, NLMMO-1/4, and

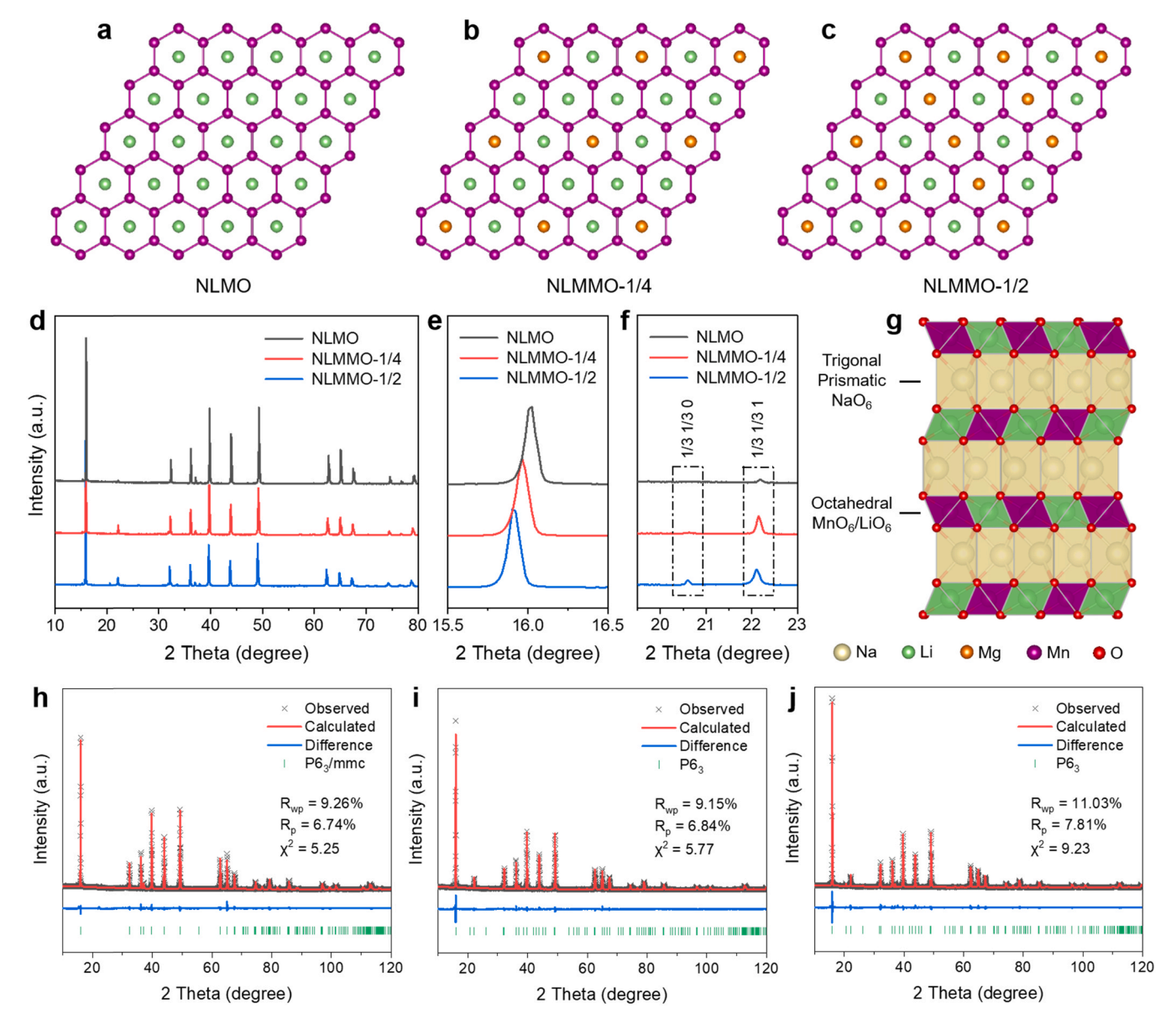


Fig. 1. Structures of NLMO and NLMMOs. Schematic illustration of in-plane structures of a) NLMO, b) NLMMO-1/4 and c) NLMMO-1/2. d) XRD patterns of NLMO, NLMMO-1/4 and NLMMO-1/2. Corresponding Rietveld refinement results are shown in (h), (i) and (j), respectively. Enlarged figures of Bragg peaks in the 2 theta range of e) 15.5°-16.5° and f) 19.5°-23°. g) Crystal structure of the layered P2-type NLMO.

NLMMO-1/2 were 203 mAh g $^{-1}$, 179 mAh g $^{-1}$, and 176 mAh g $^{-1}$, corresponding to coulombic efficiencies of 91%, 94%, and 104%, respectively. The low coulombic efficiency for O redox involved cathodes during the first charge is mainly ascribed to the irreversible O loss [30–32]. For now, the relatively higher initial coulombic efficiencies in NLMMOs can be tentatively attributed to less O loss, likely owing to the incorporation of Mg@Mn $_6$ SMs. Further discharging the cell to 1.5 V resulted in higher capacities of 262 mAh g $^{-1}$, 235 mAh g $^{-1}$, and 220 mAh g $^{-1}$ for NLMO, NLMMO-1/4, and NLMMO-1/2, respectively. It is notable that even 220 mAh g $^{-1}$ is a high capacity for Na-layered oxides.

The incorporation of $Mg@Mn_6$ SMs also led to the elevated voltage plateau of O oxidation (Fig. 2a), indicating an altered O oxidation behavior. To quantificationally investigate the effect of $Mg@Mn_6$ SMs on the O oxidation behavior, density functional theory (DFT) calculations are employed for the O 2p density of states (DOS) in both NLMO and NLMMO-1/2. As shown in Fig. S3, the O 2p band is lowered by 1.37 eV after the incorporation of $Mg@Mn_6$ SMs, which explains the higher onset voltage for O oxidation in NLMMOs. This trend can be also

observed in the cyclic voltammetry (CV) curves (Fig. 2b), in which the oxidation peaks during the first charge shift to higher voltages and become narrower with the increase of $Mg@Mn_6$ SMs. Besides, the oxidation peak during the first charge is not considered to be a neat O redox single peak. Since Mn oxidation also contributes for minor capacity during the initial charge, the minor shoulder peak before the major O redox peak can be ascribed to the oxidation of Mn.

Since oxygen loss is an irreversible process, the resultant capacity decay can accumulate during repeated charge/discharge. The cycling performance of the three materials were evaluated and compared. As shown in Fig. 2c, capacity retentions over 50 cycles were calculated to be 31%, 50% and 62% for NLMO, NLMMO-1/4 and NLMMO-1/2, respectively. Although the initial capacity of NLMO was the highest (262 mAh g⁻¹), it underwent a severe capacity degradation to only 82 mAh g⁻¹ after 50 cycles (Fig. 2d). By contrast, NLMMO-1/2 with abundant Mg@Mn₆ SMs exhibited conspicuously improved cycling stability (137 mAh g⁻¹ after 50 cycles, Fig. 2e). The capacity decay of NLMMO-1/2 can be attributed to the Mn dissolution issue, which is widely existed in Mn-based cathode materials, especially when cycled

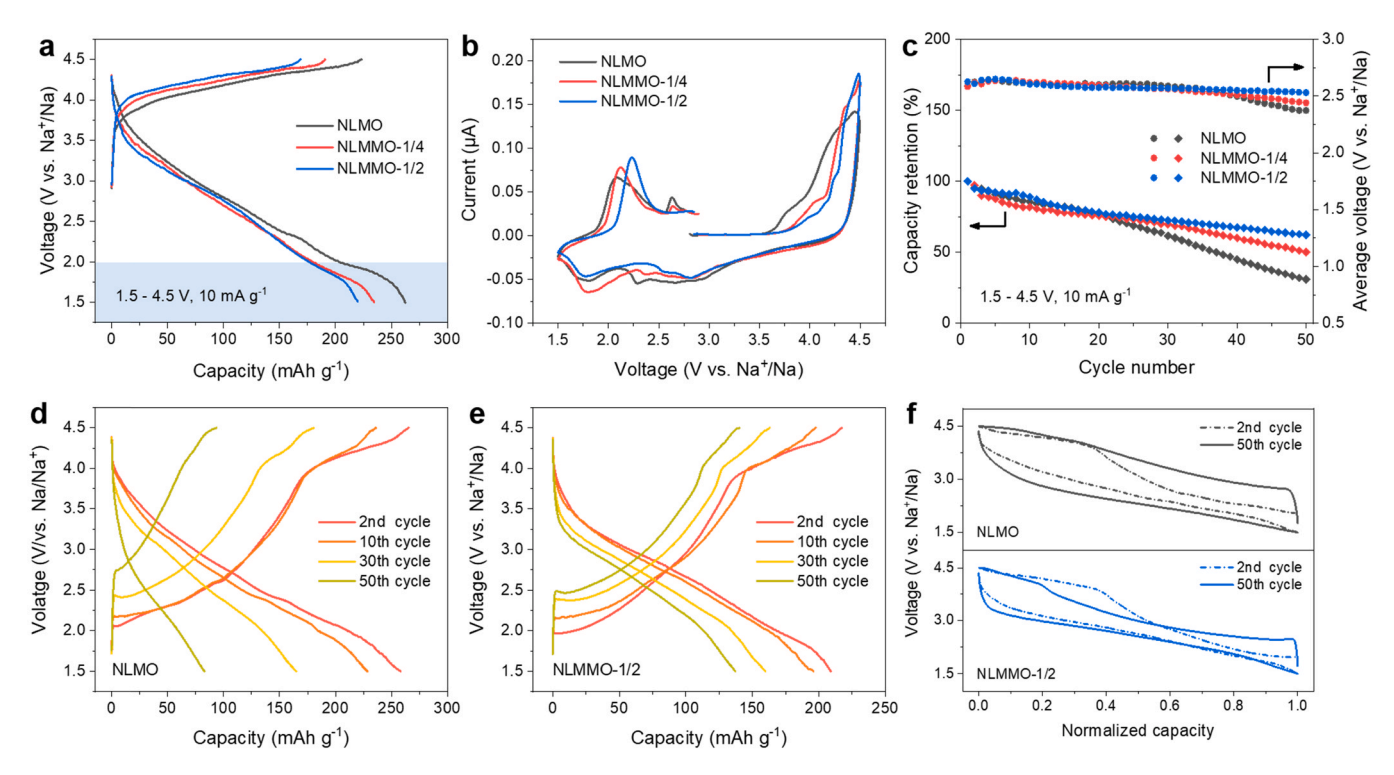


Fig. 2. Electrochemical performance of NLMO and NLMMOs. a) First-cycle charge/discharge profiles of NLMO, NLMMO-1/4 and NLMMO-1/2 when cycled between 1.5 and 4.5 V at 10 mA g $^{-1}$. b) Cyclic voltammetry curves of NLMO, NLMMO-1/4 and NLMMO-1/2 at a scan rate of 0.1 mV s $^{-1}$ between 1.5 and 4.5 V during the initial cycle. c) Capacity and voltage retention of NLMO, NLMMO-1/4 and NLMMO-1/2 when cycled between 1.5 and 4.5 V at 10 mA g $^{-1}$. Charge/discharge profiles of d) NLMO and e) NLMMO-1/2 at the 2nd, 10th, 30th and 50th cycles. f) Normalized charge/discharge profiles of NLMO and NLMMO-1/2 at the 2nd and 50th cycles.

under low voltages. Furthermore, the voltage decay issue that has been plaguing most O redox involved cathode materials was also mitigated in NLMMOs. As seen in Fig. 2c, the average voltage decays over 50 cycles are 216 mV, 143 mV, and 96 mV for NLMO, NLMMO-1/4, and NLMMO-1/2, respectively. The mitigated voltage decay is more evident in the comparison of normalized charge/discharge profiles of NLMO and NLMMO-1/2 at the 2nd and 50th cycles (Fig. 2f). In summary, the electrochemical experimental results confirm that the incorporation of a more stable second SM into the originally unstable superstructure can improve the coulombic efficiency and cycling stability of the Na-layered oxide cathodes.

2.3. Structural evolution and O loss behaviors of NLMO and NLMMOs

In order to establish the correlation between the electrochemical reversibility and the atomic-level understanding of SMs, the structural evolution during charge/discharge was thoroughly investigated. Here, XRD was employed to capture the structural evolutions upon cycling for all three materials. The corresponding XRD patterns for NLMO, NLMMO-1/4, and NLMMO-1/2 electrodes are shown in Fig. 3a, c and e, respectively. It is both interesting and surprising to find that all three materials still maintain the characteristic diffraction patterns of P2-type Na-layered oxides even after 50 cycles, although marked capacity degradations already took place (Fig. 2c). Further examination on the superlattice peaks (Fig. 3b, d, f) reveals more detailed structural information. As shown in Fig. 3b, the (1/3, 1/3, 1) peak of pristine NLMO completely disappeared after the first cycle. The loss of superlattice peaks can be either originated from the loss of honeycomb ordering or from the formation of stacking faults. However, the latter is excluded through employing the electron diffraction (ED) technique (Fig. S4). Therefore, the loss of TM ordering should account for the loss of superlattice peaks. During the first charge, both the inter-plane Li⁺ migration and the in-plane Mn⁴⁺ migration took places in NLMO [26].

As a consequence, the original honeycomb ordering of Mn ions was destroyed, resulting in the disappearance of superlattice peaks after the first charge. By contrast, the superlattice peaks of NLMMO-1/4 were retained for 20 cycles (Fig. 3d), indicating an improved structural stability. Furthermore, when half of the SM sites were occupied by the Mg@Mn₆ SMs, NLMMO-1/2 showed exceptional structural stability, with superlattice peaks still clearly visible even after 50 cycles (Fig. 3f), corresponding to the significantly improved cycling stability. The robust superstructure of NLMMO-1/2 can be attributed to the pinning effect of the stable Mg@Mn₆ SMs, which function as obstacles and inherently retard the in-plane migration of Mn ions.

With the in-plane migration of Mn ions, an inevitable result is the clustering of vacancies in the TM layer, resulting in the formation of uncoordinated O and subsequent O loss [26,33]. In this work, evolution of gas-phase oxygen was directly measured using in-situ differential electrochemical mass spectroscopy (DEMS) during the first charge. As shown in Fig. 3g, an obvious O2 signal was detected in NLMO with an onset voltage of 4.5 V, while no O₂ signal was detected in NLMMO-1/2 even at 4.8 V. Considering that the CV is a dynamical test with the voltage above 4.5 V for only a short period of time, the O2 evolution in NLMO could be considerable when galvanostatically charged to 4.5 V. Besides, the generation of CO2 is associated with the side reactions between the oxidized O species and the vulnerable electrolyte components. Although CO2 signals were detected in both materials, the amount of CO₂ evolved from NLMMO-1/2 was negligible compared with NLMO. Therefore, it is evident that the incorporation of the Mg@Mn₆ SM inherently inhibited the formation of the uncoordinated O, in accordance with the theoretical analysis based on XRD results.

2.4. Structural integrity of NLMO and NLMMOs

In order to investigate the destructive effect of O loss on the structure of the cathode materials, XPS and high-resolution transmission electron

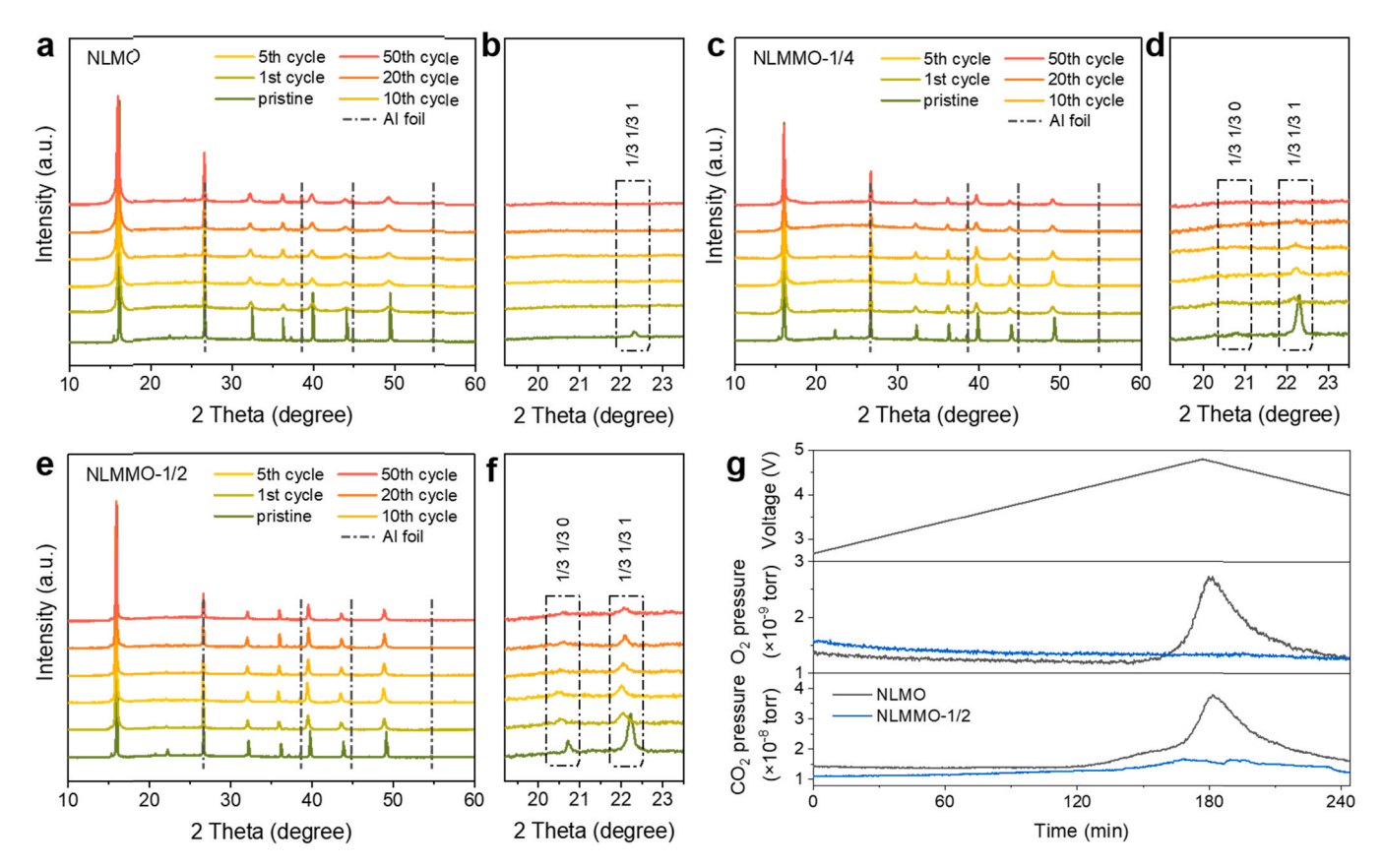


Fig. 3. Structural evolution and O loss behaviors of NLMO and NLMMOs. Evolution of XRD patterns of a) NLMO, c) NLMMO-1/4 and e) NLMMO-1/2 upon cycling. Enlarged figures of superlattice peaks are shown in (b), (d) and (f), respectively. g) In-situ differential electrochemical mass spectroscopy measurements for NLMO and NLMMO-1/2 with a scan rate of 0.2 mV s^{-1} from open circuit voltage to 4.8 V.

microscope (HRTEM) were employed to examine NLMO and NLMMO-1/2 after cycling test. The XPS Mn 2p spectra and fitting results of NLMO and NLMMO-1/2 are plotted in Fig. 4a and b, respectively. The corresponding average valence state of Mn derived from the XPS fitting results are shown in Fig. 4c. For NLMO, the initial valence state of Mn was nearly +4, and it gradually decreased to +3.65, +3.38, and + 3.34 after 10, 20, and 50 cycles, respectively. The decrease of the valence of TM is very common in O redox involved layered oxides as a consequence of the irreversible O loss, in order for charge compensation [34,35]. Therefore, it can be speculated from the XPS results that O loss continuously plagued NLMO during the first 20 cycles. After 20 cycles, the valence state of Mn became stable probably because of the depletion of unstable O in the lattice. By contrast, NLMMO-1/2 exhibited much more stable Mn valence during the whole 50 cycles. The initial valence state of Mn in NLMMO-1/2 was + 3.79 and only changed slightly to + 3.76, + 3.74, and + 3.66 after 10, 20, and 50 cycles, respectively. This mild valence drop suggests the negligible O loss in NLMMO-1/2 (Fig. 3g).

The local structures of NLMO and NLMMO-1/2 were further inspected by HRTEM. Defect-free layered structures can be identified in both NLMO and NLMMO-1/2 before being cycled (Fig. S5). After 10 cycles, micro-cracks can be identified in NLMO (Fig. 4d) while the structure of NLMMO-1/2 remained intact (Fig. 4g). The cracks in NLMO can be correlated to the broadening of the diffraction peaks in the XRD patterns, as quantified by the full width at half maxima (FWHM) of the characteristic (002), (010) and (012) peaks (Tables S5-S6 and Fig. S6). Since the increased FWHM usually suggests the decreased crystallinity, the more significant peak broadening of NLMO than NLMMO-1/2 indicates that a more drastic structural disordering took place during the initial cycle (Fig. S6). Further inspection on the crystal structure of NLMO shows seriously distorted crystal lattice and disordering regions

around the cracks (Fig. 4e). These cracks extend far to the surface (Fig. 4f), making the bulk vulnerable to the attack by the electrolyte components. Besides, a disordered layer with a thickness of ~ 8 nm can be found on the particle surface (Fig. 4f). These disordered regions either in the bulk or on the surface can be attributed to the severe O loss (Fig. 3g) and the resultant structural collapse [33,36,37]. By contrast, NLMMO-1/2 maintained excellent structural integrity with the intact layered structure both in the bulk and on the surface (Fig. 4h, i). The improved structural integrity should account for the enhanced cycling performance of NLMMOs.

2.5. Regulating the superstructural motifs

Based on the results above, the expected scenario is schematically illustrated in Fig. 5. The theoretical evolution of the NLMO structure after charging is visualized. As seen in Fig. 5a, there is only one type of SM in NLMO, Li@Mn₆, in which each O^2 is coordinated with one Li⁺ and two Mn ions (Fig. 5d) [7]. Due to the weak electrostatic attraction between Li⁺ and O^2 , O^2 in this local coordination environment (LCE) has a higher electronic density, or a higher O 2p (Na-O-Li) state in the DOS, than those coordinated with three TMs (Fig. 5e) [38]. Upon charging, the Li-coordinated O^2 experiences an oxidation reaction. On the other hand, the weak Li⁺- O^2 interaction also endows Li⁺ with high mobility, allowing Li⁺ migrate away from the TM layer to the AM layer under deep charge (Fig. 5b) [25,26]. The vacancies left in the TM layer tend to cluster forming pores with O_2 inside (Fig. 5c). As gaseous oxygen escapes from the material, pores remain and the loss of the oxygen from the structure is irreversible.

Therefore, precluding vacancies from clustering is the key to inherently inhibit O loss, which requires a chemically inactive SM with low ion mobility in the structure. As a demonstration, the $Mg@Mn_6$ SM is

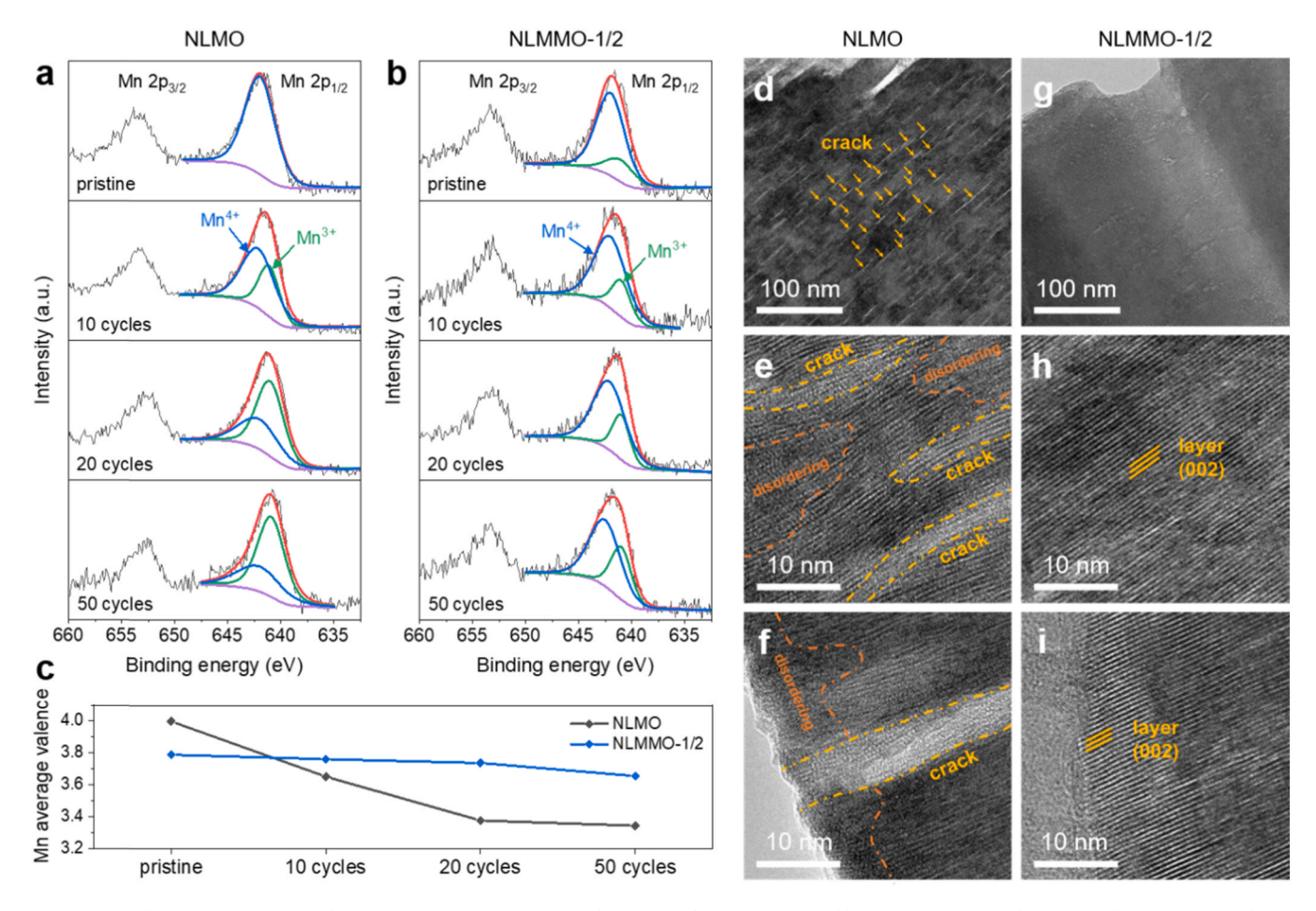


Fig. 4. Structural integrity of NLMO and NLMMOs. XPS Mn 2p spectra and fitting results of a) NLMO and b) NLMMO-1/2 after different cycles. c) Average valence of Mn derived from XPS results. High resolution transmission electron microscope (HRTEM) images of d, g) particle morphologies, e, h) bulk structures and f, i) surface structures for NLMO and NLMMO-1/2 after 10 cycles.

selected on purpose because Mg²⁺ has stronger ionic interaction with O²⁻ and therefore should meet the requirement. In this work, the honeycomb superstructure is reserved while some of the less stable Li@Mn₆ SMs are replaced by the stable Mg@Mn6. The resulted NLMMO contains both Li@Mn₆ and Mg@Mn₆ SMs (Fig. 5h), with O²⁻ in different LCEs. Specifically, in the Mg@Mn₆ SM, O²⁻ is coordinated by one Mg²⁺ and two Mn ions (Fig. 5f) [13,39]. Since the strength of the Mg^{2+} - O^{2-} interaction is between those of the Li⁺-O²⁻ interaction and the Mn⁴⁺-O²⁻ interaction, the O 2p (Na-O-Mg) state of O2- in the Mg@Mn6 SM is situated between those of the other two configurations of O²- (Na-O-Li and Na-O-Mn) in the DOS (Fig. 5g). Consequently, the redox activity of O and capacity of Na in NLMMO should be lower than those of NLMO. However, the relatively stronger interaction between Mg²⁺ and O²⁻ is expected to fix Mg²⁺ in place to retain the in-plane structure of the TM layer (Fig. 5i) [40]. These stagnant Mg@Mn6 SMs function as obstacles to TM migration and the gathering of vacancies, and thus inherently inhibit the formation of uncoordinated O (Fig. 5j). Thus far, the complete logical chain from the atomic-level understanding of SMs to the macroscopical electrochemical performance is established, demonstrating the effectiveness of the SM regulating strategy.

This SM regulating strategy might also potentially affect the redox heterogeneity at the mesoscale [41,42]. In O-redox cathodes, irreversible O loss leads to decreased O redox reactions and consequently increased TM redox reactions (especially Mn redox reactions in this work). Since irreversible O loss usually originates from surface vicinity and gradually propagates into the interior of particle, there can be a

naturally formed redox gradient for both O and TM, with more TM redox reactions in the surface vicinity but more O redox reactions in the bulk, exhibiting redox heterogeneity. With our doping strategy, O loss can be inherently inhibited. Therefore, the redox behavior can be more homogeneous throughout the particle.

3. Conclusions

In summary, we demonstrated a universal strategy to address the O loss issue in anionic redox cathodes by directionally regulating the SMs. Based on the understanding of intrinsic chemical properties of SMs, appropriate SMs are selected to yield target performance in anionic redox cathodes. As a demonstration, by partially replacing the unstable Li@Mn₆ SMs with the more stable Mg@Mn₆ SMs, the resulted NLMMOs with regulated superstructures can harness the anionic redox for extra capacity with stable reversibility and thus exhibited significantly improved cycling performance. The inherent mechanism is explained by the pinning effect of the Mg@Mn₆ SMs, deriving from the strong Mg²⁺-O²⁻ interaction. The Mg@Mn₆ SMs serve as obstacles and inherently retard the in-plane migration of Mn ions, as well as the resultant formation of uncoordinated O and the consequent irreversible O loss. The inhibition of O loss ensures the structural integrity of NLMMO, which finally accounts for the improved cycling stability. We revealed that the structural stability can be tailored through SM regulation and it is directly related to the reversibility of anionic redox reactions. This strategy can be further expanded by employing variable SMs and be

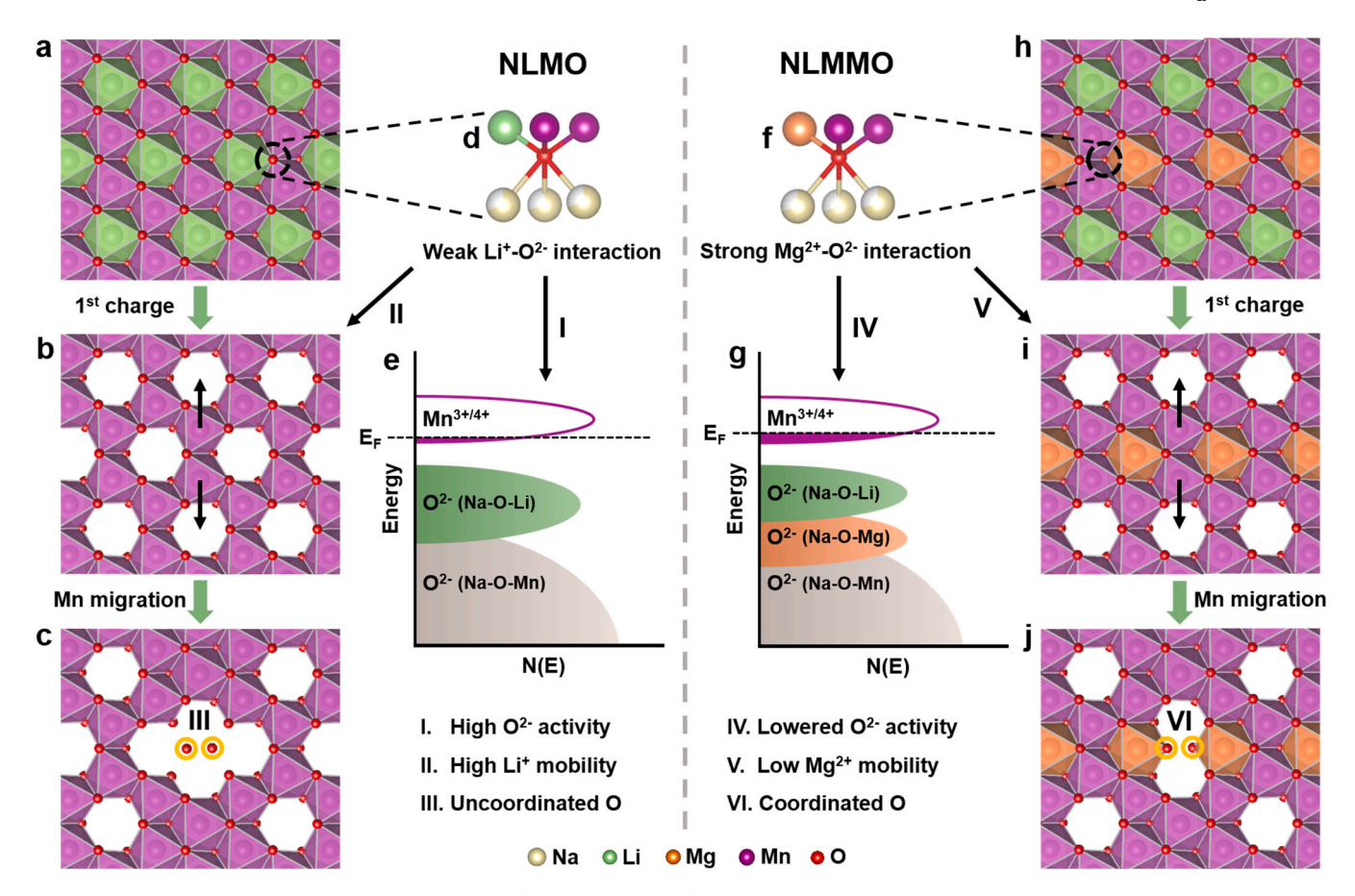


Fig. 5. Expected scenario in NLMO and NLMMO. Schematic illustration of the in-plane structural evolutions of a-c) NLMO and h-j) NLMMO during the first charge. Local coordination environments of O²⁻ in d) NLMO and f) NLMMO. Schematic illustrations for O 2p DOS in e) NLMO and g) NLMMO.

applied universally to other intercalation cathodes where the anionic redox related structural motifs are present, inspiring the design and development of next-generation high energy cathodes for future batteries.

CRediT authorship contribution statement

Jiajie Liu: Methodology, Formal analysis, Writing - original draft. Rui Qi: Conceptualization, Investigation, Visualization, Formal analysis. Changjian Zuo: Investigation. Cong Lin: Formal analysis. Wenguang Zhao: Investigation. Ni Yang: Investigation. Jianyuan Li: Investigation. Junliang Lu: Investigation. Xin Chen: Investigation. Jimin Qiu: Investigation. Mihai Chu: Resources. Mingjian Zhang: Resources. Cheng Dong: Funding acquisition. Yinguo Xiao: Resources. Haibiao Chen: Writing - review & editing. Feng Pan: Writing - review & editing, Supervision, Project administration, Funding acquisition.

Declaration of Competing Interest

The authors declare that they have no known competing financial interests or personal relationships that could have appeared to influence the work reported in this paper.

Acknowledgements

This work gratefully acknowledges support from the National Key R&D Program of China (2016YFB0700600), Shenzhen Science and Technology Research Grant (No. JCYJ20200109140416788), Chemistry and Chemical Engineering Guangdong Laboratory (Grant No. 1922018)

and National Key R&D Program of China (2020YFB0704500).

Appendix A. Supporting information

Supplementary data associated with this article can be found in the online version at doi:10.1016/j.nanoen.2021.106252.

References

- J.Y. Hwang, S.T. Myung, Y.K. Sun, Sodium-ion batteries: present and future, Chem. Soc. Rev. 46 (2017) 3529–3614.
- [2] C. Vaalma, D. Buchholz, M. Weil, S. Passerini, A cost and resource analysis of sodium-ion batteries, Nat. Rev. Mater. 3 (2018) 18013.
- [3] M.H. Han, E. Gonzalo, G. Singh, T. Rojo, A comprehensive review of sodium layered oxides: powerful cathodes for Na-ion batteries, Energy Environ. Sci. 8 (2015) 81–102.
- [4] Q. Wang, S. Mariyappan, J. Vergnet, A.M. Abakumov, G. Rousse, F. Rabuel, M. Chakir, J.-M. Tarascon, Reaching the energy density limit of layered O3-NaNi_{0.5}Mn_{0.5}O₂ electrodes via dual Cu and Ti substitution, Adv. Energy Mater. 9 (2019), 1901785.
- [5] W. Li, E.M. Erickson, A. Manthiram, High-nickel layered oxide cathodes for lithium-based automotive batteries, Nat. Energy 5 (2020) 26–34.
- [6] Q. Liu, Z. Hu, W. Li, C. Zou, H. Jin, S. Wang, S. Chou, S.-X. Dou, Sodium transition metal oxides: the preferred cathode choice for future sodium-ion batteries, Energy Environ. Sci. 14 (2021) 158–179.
- [7] N. Yabuuchi, R. Hara, M. Kajiyama, K. Kubota, T. Ishigaki, A. Hoshikawa, S. Komaba, New O2/P2-type Li-excess layered manganese oxides as promising multi-functional electrode materials for rechargeable Li/Na batteries, Adv. Energy Mater. 4 (2014), 1301453.
- [8] X. Rong, J. Liu, E. Hu, Y. Liu, Y. Wang, J. Wu, X. Yu, K. Page, Y.-S. Hu, W. Yang, H. Li, X.-Q. Yang, L. Chen, X. Huang, Structure-induced reversible anionic redox activity in Na layered oxide cathode, Joule 2 (2018) 125–140.
- [9] X. Rong, E. Hu, Y. Lu, F. Meng, C. Zhao, X. Wang, Q. Zhang, X. Yu, L. Gu, Y.-S. Hu, H. Li, X. Huang, X.-Q. Yang, C. Delmas, L. Chen, Anionic redox reaction-induced

- high-capacity and low-strain cathode with suppressed phase transition, Joule 3 (2019) 503–517.
- [10] C. Zhao, Q. Wang, Z. Yao, J. Wang, B. Sánchez-Lengeling, F. Ding, X. Qi, Y. Lu, X. Bai, B. Li, H. Li, A. Aspuru-Guzik, X. Huang, C. Delmas, M. Wagemaker, L. Chen, Y.-S. Hu, Rational design of layered oxide materials for sodium-ion batteries, Science 370 (2020) 708–711.
- [11] Q. Wang, S. Mariyappan, G. Rousse, A.V. Morozov, B. Porcheron, R. Dedryvère, J. Wu, W. Yang, L. Zhang, M. Chakir, M. Avdeev, M. Deschamps, Y.-S. Yu, J. Cabana, M.-L. Doublet, A.M. Abakumov, J.-M. Tarascon, Unlocking anionic redox activity in O3-type sodium 3d layered oxides via Li substitution, Nat. Mater. 20 (2021) 353–361.
- [12] D.-H. Seo, J. Lee, A. Urban, R. Malik, S. Kang, G. Ceder, The structural and chemical origin of the oxygen redox activity in layered and cation-disordered Liexcess cathode materials, Nat. Chem. 8 (2016) 692–697.
- [13] N. Yabuuchi, R. Hara, K. Kubota, J. Paulsen, S. Kumakura, S. Komaba, A new electrode material for rechargeable sodium batteries: P2-type Na_{2/3}[Mg_{0.28}Mn_{0.72}] O₂ with anomalously high reversible capacity, J. Mater. Chem. A 2 (2014) 16851–16855.
- [14] B. Song, E. Hu, J. Liu, Y. Zhang, X.-Q. Yang, J. Nanda, A. Huq, K. Page, A novel P3-type Na_{2/3}Mg_{1/3}Mn_{2/3}O₂ as high capacity sodium-ion cathode using reversible oxygen redox, J. Mater. Chem. A 7 (2019) 1491–1498.
- [15] A. Konarov, J.H. Jo, J.U. Choi, Z. Bakenov, H. Yashiro, J. Kim, S.-T. Myung, Exceptionally highly stable cycling performance and facile oxygen-redox of manganese-based cathode materials for rechargeable sodium batteries, Nano Energy 59 (2019) 197–206.
- [16] X. Bai, M. Sathiya, B. Mendoza-Sánchez, A. Iadecola, J. Vergnet, R. Dedryvère, M. Saubanère, A.M. Abakumov, P. Rozier, J.-M. Tarascon, Anionic redox activity in a newly Zn-doped sodium layered oxide P2-Na_{2/3}Mn_{1-y}Zn_yO₂ (0<y<0.23), Adv. Energy Mater. 8 (2018), 1802379.</p>
- [17] Q. Wang, W. Yang, F. Kang, B. Li, Na₂Mn³⁺_{0.3}Mn⁴⁺_{2.7}O_{6.85}: a cathode with simultaneous cationic and anionic redox in Na-ion battery, Energy Storage Mater. 14 (2018) 361–366.
- [18] C. Zhao, Q. Wang, Y. Lu, L. Jiang, L. Liu, X. Yu, L. Chen, B. Li, Y.-S. Hu, Decreasing transition metal triggered oxygen redox activity in Na-deficient oxides, Energy Storage Mater. 20 (2019) 395–400.
- [19] Y. Li, X. Wang, Y. Gao, Q. Zhang, G. Tan, Q. Kong, S. Bak, G. Lu, X.-Q. Yang, L. Gu, J. Lu, K. Amine, Z. Wang, L. Chen, Native vacancy enhanced oxygen redox reversibility and structural robustness, Adv. Energy Mater. 9 (2019), 1803087.
- [20] S. Sharifi-Asl, J. Lu, K. Amine, R. Shahbazian-Yassar, Oxygen release degradation in Li-ion battery cathode materials: mechanisms and mitigating approaches, Adv. Energy Mater. 9 (2019), 1900551.
- [21] J. Hong, H.-D. Lim, M. Lee, S.-W. Kim, H. Kim, S.-T. Oh, G.-C. Chung, K. Kang, Critical role of oxygen evolved from layered Li–excess metal oxides in lithium rechargeable batteries, Chem. Mater. 24 (2012) 2692–2697.
- [22] W. Yang, Oxygen release and oxygen redox, Nat. Energy 3 (2018) 619–620.
- [23] E. Zhao, M. Zhang, X. Wang, E. Hu, J. Liu, X. Yu, M. Olguin, T.A. Wynn, Y.S. Meng, K. Page, F. Wang, H. Li, X.-Q. Yang, X. Huang, L. Chen, Local structure adaptability through multi cations for oxygen redox accommodation in Li-rich layered oxides, Energy Storage Mater. 24 (2020) 384–393.
- [24] W.E. Gent, K. Lim, Y. Liang, Q. Li, T. Barnes, S.-J. Ahn, K.H. Stone, M. McIntire, J. Hong, J.H. Song, Y. Li, A. Mehta, S. Ermon, T. Tyliszczak, D. Kilcoyne, D. Vine, J.-H. Park, S.-K. Doo, M.F. Toney, W. Yang, D. Prendergast, W.C. Chueh, Coupling between oxygen redox and cation migration explains unusual electrochemistry in lithium-rich layered oxides, Nat. Commun. 8 (2017) 2091.
- [25] R.A. House, G.J. Rees, M.A. Pérez-Osorio, J.-J. Marie, E. Boivin, A.W. Robertson, A. Nag, M. Garcia-Fernandez, K.-J. Zhou, P.G. Bruce, First-cycle voltage hysteresis in Li-rich 3d cathodes associated with molecular O₂ trapped in the bulk, Nat. Energy 5 (2020) 777-785.
- [26] R.A. House, U. Maitra, M.A. Pérez-Osorio, J.G. Lozano, L. Jin, J.W. Somerville, L. C. Duda, A. Nag, A. Walters, K.-J. Zhou, M.R. Roberts, P.G. Bruce, Superstructure control of first-cycle voltage hysteresis in oxygen-redox cathodes, Nature 577 (2020) 502–508.
- [27] X.-L. Li, T. Wang, Y. Yuan, X.-Y. Yue, Q.-C. Wang, J.-Y. Wang, J. Zhong, R.-Q. Lin, Y. Yao, X.-J. Wu, X.-Q. Yu, Z.-W. Fu, Y.-Y. Xia, X.-Q. Yang, T. Liu, K. Amine, Z. Shadike, Y.-N. Zhou, J. Lu, Whole-voltage-range oxygen redox in P2-layered cathode materials for sodium-ion batteries, Adv. Mater. 33 (2021), 2008194.
- [28] Q.-C. Wang, J.-K. Meng, X.-Y. Yue, Q.-Q. Qiu, Y. Song, X.-J. Wu, Z.-W. Fu, Y.-Y. Xia, Z. Shadike, J. Wu, X.-Q. Yang, Y.-N. Zhou, Tuning P2-structured cathode material by Na-site Mg substitution for Na-ion batteries, J. Am. Chem. Soc. 141 (2019) 840–848.
- [29] P.-F. Wang, Y. You, Y.-X. Yin, Y.-S. Wang, L.-J. Wan, L. Gu, Y.-G. Guo, Suppressing the P2-O2 phase transition of Na_{0.67}Mn_{0.67}Ni_{0.33}O₂ by magnesium substitution for improved sodium-ion batteries, Angew. Chem. Int. Ed. Engl. 55 (2016) 7445–7449.
- [30] A. Manthiram, J.C. Knight, S.-T. Myung, S.-M. Oh, Y.-K. Sun, Nickel-rich and lithium-rich layered oxide cathodes: progress and perspectives, Adv. Energy Mater. 6 (2016), 1501010.
- [31] J. Zheng, S. Myeong, W. Cho, P. Yan, J. Xiao, C. Wang, J. Cho, J.-G. Zhang, Li- and Mn-rich cathode materials: challenges to commercialization, Adv. Energy Mater. 7 (2017), 1601284.
- [32] P.K. Nayak, E.M. Erickson, F. Schipper, T.R. Penki, N. Munichandraiah, P. Adelhelm, H. Sclar, F. Amalraj, B. Markovsky, D. Aurbach, Review on challenges and recent advances in the electrochemical performance of high capacity Li- and Mn-rich cathode materials for Li-ion batteries, Adv. Energy Mater. 8 (2018), 1702397.
- [33] R.A. House, U. Maitra, L. Jin, J.G. Lozano, J.W. Somerville, N.H. Rees, A.J. Naylor, L.C. Duda, F. Massel, A.V. Chadwick, S. Ramos, D.M. Pickup, D.E. McNally, X. Lu,

- T. Schmitt, M.R. Roberts, P.G. Bruce, What triggers oxygen loss in oxygen redox cathode materials, Chem. Mater. 31 (2019) 3293–3300.
- [34] J. Wu, Z. Zhuo, X. Rong, K. Dai, Z. Lebens-Higgins, S. Sallis, F. Pan, L.F.J. Piper, G. Liu, Y.-D. Chuang, Z. Hussain, Q. Li, R. Zeng, Z.-X. Shen, W. Yang, Dissociate lattice oxygen redox reactions from capacity and voltage drops of battery electrodes, Sci. Adv. 6 (2020) 3871.
- [35] E. Hu, X. Yu, R. Lin, X. Bi, J. Lu, S. Bak, K.-W. Nam, H.L. Xin, C. Jaye, D.A. Fischer, K. Amine, X.-Q. Yang, Evolution of redox couples in Li- and Mn-rich cathode materials and mitigation of voltage fade by reducing oxygen release, Nat. Energy 3 (2018) 690–698.
- [36] P. Yan, J. Zheng, M. Gu, J. Xiao, J.-G. Zhang, C.-M. Wang, Intragranular cracking as a critical barrier for high-voltage usage of layer-structured cathode for lithium-ion batteries, Nat. Commun. 8 (2017) 14101.
- [37] P. Yan, J. Zheng, Z.-K. Tang, A. Devaraj, G. Chen, K. Amine, J.-G. Zhang, L.-M. Liu, C. Wang, Injection of oxygen vacancies in the bulk lattice of layered cathodes, Nat. Nanotechnol. 14 (2019) 602–608.
- [38] K. Luo, M.R. Roberts, R. Hao, N. Guerrini, D.M. Pickup, Y.-S. Liu, K. Edström, J. Guo, A.V. Chadwick, L.C. Duda, P.G. Bruce, Charge-compensation in 3d-transition-metal-oxide intercalation cathodes through the generation of localized electron holes on oxygen, Nat. Chem. 8 (2016) 684–691.
- [39] K. Dai, J. Wu, Z. Zhuo, Q. Li, S. Sallis, J. Mao, G. Ai, C. Sun, Z. Li, W.E. Gent, W. C. Chueh, Y.-D. Chuang, R. Zeng, Z.-X. Shen, F. Pan, S. Yan, L.F.J. Piper, Z. Hussain, G. Liu, W. Yang, High reversibility of lattice oxygen redox quantified by direct bulk probes of both anionic and cationic redox reactions, Joule 3 (2019) 518–541.
- [40] U. Maitra, R.A. House, J.W. Somerville, N. Tapia-Ruiz, J.G. Lozano, N. Guerrini, R. Hao, K. Luo, L. Jin, M.A. Perez-Osorio, F. Massel, D.M. Pickup, S. Ramos, X. Lu, D.E. McNally, A.V. Chadwick, F. Giustino, T. Schmitt, L.C. Duda, M.R. Roberts, P. G. Bruce, Oxygen redox chemistry without excess alkali-metal ions in Na_{2/3}[Mg_{0.28}Mn_{0.72}]O₂, Nat. Chem. 10 (2018) 288–295.
- [41] J. Zhang, Q. Wang, S. Li, Z. Jiang, S. Tan, X. Wang, K. Zhang, Q. Yuan, S.-J. Lee, C. J. Titus, K.D. Irwin, D. Nordlund, J.-S. Lee, P. Pianetta, X. Yu, X. Xiao, X.-Q. Yang, E. Hu, Y. Liu, Depth-dependent valence stratification driven by oxygen redox in lithium-rich layered oxide, Nat. Commun. 11 (2020) 6342.
- [42] C. Wei, S. Xia, H. Huang, Y. Mao, P. Pianetta, Y. Liu, Mesoscale battery science: the behavior of electrode particles caught on a multispectral X-ray camera, Acc. Chem. Res. 51 (2018) 2484–2492.



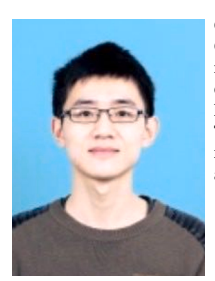
Jiajie Liu is currently a Ph.D. candidate in Prof. Feng Pan's group at Peking University Shenzhen Graduate School, China. He received his B.S. degree in Chemistry from Peking University in 2016. Currently his research interests focus on high energy density cathode materials for Li-/Na ion batteries, especially on layered oxide materials including Li- and Mn-rich layered oxides and Ni-rich layered oxides.



Rui Qi is currently pursuing his M.Sc. degree under the supervision of Prof. Feng Pan at Peking University Shenzhen Graduate School, China. He received his B.Eng. degree from Central South University in 2018. His research interests mainly focus on investigating the relation between the structure of cathode materials for Li- and Na-ion batteries and their electrochemical behavior.



Changjian Zuo graduated from Soochow university and received his B.S. degree from the School of Shangang Iron and Steel in 2018. He is currently a postgraduate student in Prof. Feng Pan's group at the school of Advanced Materials, Peking University Shenzhen Graduate School. His research interests focus on the cathode materials of lithium ion batteries.



Cong Lin received his B.S. and Ph.D. degree in chemistry from Chongqing University and Peking University in 2013 and 2018, respectively. From 2018 to early 2021, he worked as a post-doctor in Prof. Feng Pan's group in Peking University Shenzhen Graduate School, and is currently a postdoctoral fellow in The Hong Kong Polytechnic University. His research interest mainly focuses on the structures of novel functional materials and their relationship with properties and performances.



Xin Chen is currently a postgraduate student in Prof. Feng Pan's group at the School of Advanced Materials, Peking University, Shenzhen Graduate School. He received his B.S. in School of Materials Science and Engineering, Central South University, China. His research mainly focuses on theoretical calculation and design of advanced materials.



Wenguang Zhao is an engineer in the School of Advanced Materials, Peking University Shenzhen Graduate School, China. He has over 10 years' experience in material characterization using wide range of analytical tools including XRD, XPS, SEM and TEM. His research interests mainly focus on the Ex/in-situ TEM and Ex/in-situ XRD characterization of battery materials



Jimin Qiu received his Bachelor's degree in 2020 from College of Chemistry and Chemical Engineering, Xiamen University, China. His is now a postgraduate student in the School of Advanced Materials, Peking University, Shenzhen Graduate School, China. His research interests focus on Li/Na layered transition metal oxide cathodes.



Ni Yang is an engineer in the school of Advanced Materials, Peking University Shenzhen Graduate School, China. She has sufficient experience in the preparation of transmission samples and her research focuses on using 3D reconstruction to study battery materials.



Mihai Chu received his B.Eng. degree from the School of Optical and Electronic Information at Huazhong University of Science and Technology in 2017. He is currently pursuing his master degree in the School of Advanced Materials, Peking University under the supervision of Prof. Yinguo Xiao. His research interests mainly focus on the synthesis of cathode materials and the structural characterization based on X-ray and neutron diffraction methods.



Jianyuan Li received his B.S. degree from School of Chemistry and Chemical Engineering, Shandong University, China in 2017. He is currently a Ph.D. candidate in School of Advanced Material, Peking University, China. His research interests focus on the structure evolution and characterization of battery materials.



Mingjian Zhang got his Ph.D. degree from Fujian Institute of Research on the Structure of Matter, Chinese Academy of Sciences in 2013, then worked there as an assistant research fellow for one year. From 2014–2018, he was a postdoc in School of Advanced Materials, Peking University, and became an assistant/associate research professor since 2018. Meanwhile, he was a research scholar in Brookhaven National Lab from 2016 to 2019, then in the University of Chicago since 2019. He has been engaged in the fields of electrode materials for Li-ion batteries, crystal growth and structure analysis of nonlinear optical crystals.



Junliang Lu is currently a graduate student at Feng Pan's group at Peking University Shenzhen Graduate School, China. He received his B.S. degree in Chemistry from Northwest University in 2018. His research interests mainly focus on cathode materials for lithium batteries, especially on manganese-pure oxides.



Cheng Dong received a Bachelor of Science (1981) and Master of Science (1984) from Peking University, and a Ph.D. from the Institute of Physics, Chinese Academy of Sciences (1988). From 1988–1991, he did post-doctoral research in the Department of Physics at the University of Arkansas and the University of Colorado. From 1991–2019, he worked at the State Key Laboratory of Superconductivity, Institute of Physics, Chinese Academy of Sciences. Since August 2019, he has been working in the School of Advanced Materials, Peking University Shenzhen Graduate School.



Yinguo Xiao received his Ph.D. degree from Institute of Physics, Chinese Academy of Sciences, China in 2006. He was a postdoctoral fellow from 2007 to 2009 and a research scientist from 2009 to 2014 at Juelich Research Centre (Forschungszentrum Jülich), Germany. He became a tenured staff scientist in Juelich Research Centre since 2015. In 2017, he joined Peking University Shenzhen Graduate School, China as an associate professor. His research interests are on research and development of new materials for energy conversion and storage, and characterization of complex materials using X-ray and neutron scattering techniques.



Feng Pan, founding Dean of School of Advanced Materials, Peking University Shenzhen Graduate School, got B.S. from Dept. Chemistry, Peking University in 1985 and Ph.D. from Dept. of P&A Chemistry, University of Strathclyde, Glasgow, UK, with "Patrick D. Ritchie Prize" for the best Ph.D. in 1994. With more than a decade experience in large international incorporations, Prof. Pan has been engaged in fundamental research and product development of novel optoelectronic and energy storage materials and devices. As Chief Scientist, Prof. Pan led eight entities in Shenzhen to win 150 million RMB grant for the national new energy vehicles (power battery) innovation project since 2013.



Haibiao Chen is currently a research professor at Shenzhen Polytechnic. He received his Bachelor's degree from Tsinghua University in 2000 and Ph.D. from Stevens Institute of Technology in 2006. He worked at Velocys during 2006–2011 and UES during 2011–2014. He was a senior researcher at the School of Advanced Materials, Peking University Shenzhen Graduate School from 2014 to 2020.